UNIVERSITY OF CINCINNATI

Date: feb 1st, 2007

I, MURALI KRISHNA KILARU,
hereby submit this work as part of the requirements for the degree of:

in:
Electrical and Computer Engineering

It is entitled:
Hydrophobic Dielectrics of Fluoropolymer / Barium Titanate
Nanocomposites for Low-Voltage and Charge Storing Electrowetting Devices

This work and its defense approved by:

Chair: Dr. JASON HEIKENFELD
Dr. JAMES MARK
Dr. FRED BEYETTE

HYDROPHOBIC DIELECTRICS OF FLUOROPOLYMER/ BARIUM TITANATE NANOCOMPOSITES FOR LOW-VOLTAGE AND CHARGE STORING ELECTROWETTING DEVICES

A thesis submitted to the
Division of Research and Advanced Studies
of the University of Cincinnati
in partial fulfillment of requirement for the degree of

MASTER OF SCIENCE

In the Department of Electrical and Computer Engineering
of the College of Engineering
January 2007
By

Murali Krishna Kilaru

B.Tech (Electronics and Communications Engineering),
V.R. Siddhartha Engineering College, Vijayawada, A.P, India

Committee Chair: Dr. Jason Heikenfeld

ABSTRACT

Electrowetting is making a great impact in fields of optics, lab-on chip devices and electronic paper (e-paper). For electrowetting to realize its fullest potential in low operating voltage applications, solutions to some of the common material challenges need to be addressed. These challenges include electrolysis, dielectric breakdown, and surface damage at high electric fields.

This thesis paves the way for a new approach to achieve low-voltage electrowetting and improved power efficiency for electrowetting devices. This approach does not have the drawbacks such as dielectric breakdown or electrolysis. The theoretical factors leading to low-voltage electrowetting are known. One approach is to increase the permittivity (k) of the dielectric on which electrowetting occurs. However, conventional hydrophobic dielectrics such as fluoropolymers do not usually have a high dielectric constant.

This thesis provides a novel approach to increase the dielectric constant of the fluoropolymer by making a nanocomposite dielectric of fluoropolymer and high-k inorganic powder. This composite retains the hydrophobicity of the fluoropolymer and the dielectric constant of high-k powder. The compatibility of the nanocomposite dielectric to electrowetting is tested by various characterizations. Results indicate that this approach does increase dielectric constant of fluoropolymer and thereby achieves low-voltage electrowetting. Apart from these expected results, strong charge storage is observed for the composite dielectric, which could lead to new applications for electrowetting. The ability of the nanocomposite dielectric to be tailor made using

various composite materials could open up electrowetting to a variety of new research paths.

TABLE OF CONTENTS

CHAPTER 1

CHAPTER 2

CHAPTER 3

CHAPTER 4

CHAPTER 5

LIST OF FIGURES

LIST OF TABLES

CHAPTER 1

INTRODUCTION

1.1 Electrowetting

Electrowetting was first defined several decades ago as “the change in solid electrolyte contact angle due to an applied potential difference between the solid and the electrolyte” [1]. Electrowetting of an electrically conductive liquid occurs when a bias is applied between a polar liquid and an underlying dielectric coated electrode. Electrowetting is finding increasing number of applications in modern day fields. These include micro-fluidics for lab-on chip devices [2], optics [3], e-paper [4], and displays [5]. Most of these applications demand low voltage operation. Low voltage conserves power and makes electrowetting more feasible for commercial applications.

In electrowetting, it is usually desirable to have a large contact angle of the liquid when no voltage bias is applied. Therefore, a hydrophobic polymer layer is used as the top surface on the dielectric. In electrowetting, the contact angle of liquid changes as it is electrostatically attracted to the dielectric underneath. This electrostatic force is directly proportional to the capacitance of dielectrics used. Conventional hydrophobic polymers such as Teflon [6] do not have a high dielectric constant. Therefore, a common approach to achieve greater electrostatic force of attraction at lower-voltage operation has been to make the hydrophobic layer as thin (<100nm) as possible compared to dielectric thickness underneath.

This technique has many challenges. These include electrolysis of the liquid due to dielectric breakdown and irreversible damages caused to the hydrophobic surface due to electrochemical reaction of the surface at high electric fields [7]. If we are to consider other approaches that aim at lower-voltage electrowetting they need to have these challenges addressed. A simple solution would be to have thicker hydrophobic layers with higher dielectric constant. Achieving such a new material would benefit all electrowetting devices in terms of lower voltage, improved reliability, and fabrication that is less sensitive to nanoscale dielectric defects.

1.2 In this thesis

A novel technique to lower voltage in electrowetting is investigated. It has been observed that there is a lack of alternate material choices to the low-dielectric constant fluoropolymers used in electrowetting [8]. This thesis presents an inorganic/organic nanocomposite approach to achieve low-voltage electrowetting.

In this method, a high dielectric constant (high 'k') nano-powder is dispersed in fluoropolymer to prepare a nanocomposite dielectric. This would retain the hydrophobicity of fluoropolymer and the high dielectric constant of the nanopowder. The results obtained show an increase in dielectric constant, confirmed by lower-voltage electrowetting. This was also accompanied with many other interesting results like larger initial contact angle and bistable wetting. Bistable wetting implies that after the voltage is removed, the droplet is able to retain its electrowetting state until a later voltage is applied to remove the droplet from the electrowetted state. No previous reports exist for electrowetting dielectrics showing strong bistable behavior. Bistable wetting, a consequence of charge trapping could be instrumental in making the electrowetting devices very power efficient. The bistable wetting could prove critically important for emerging electrowetting applications such as e-paper.

This novel nanocomposite dielectric was developed and tested for reduced electrowetting voltage. Bistable wetting behavior was further investigated using charge-voltage analysis. These studies provide experimental proof of the proposed performance of the nanocomposite dielectric. This thesis further sets the stage for future applied work in e-paper and future fundamental work in understanding/engineering the nanocomposite charge trapping mechanism.

CHAPTER 2

THEORETCAL BACKGROUND

2.1 Contact angle at zero potential

2.1.1 Contact angle on a planar surface

A liquid droplet placed on a surface has a specific shape which is a fraction of sphere, often referred to as a spherical cap. This shape is defined by the interfacial surface tensions. Any deviation from the spherical shape is due to the effects of gravity on the droplet. The angle at which the liquid/vapor interface meets the solid surface is called the contact angle of that liquid on that surface. From this point forward in the thesis, the liquid referred to herein and that is used for electrowetting is de-ionized water. The contact angle of a water droplet on a surface is defined by Young's equation. The Young's equation gives the thermodynamic equilibrium of the 3 interfacial surface tension vectors- γ_{AF} (fluoropolymer/air), γ_{SA}(saline/air) , γ_{SF}(saline/fluoropolymer) at the triple phase contact point of water droplet as seen in fig. 2.1.

The Young's equation is achieved summing the in-plane components of these vectors and is given by equation 1.

$$\gamma_{SF} = \gamma_{AF} - \gamma_{SA} \cos\theta_o \qquad (1)$$

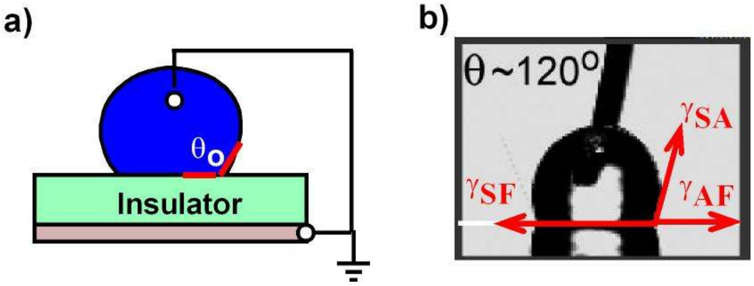

Fig 2.1, (a) Saline droplet on a fluoropolymer surface with contact angle θ_o with no voltage bias. (b) The interfacial surface tensions γ_{SA} , γ_{AF} ,γ_{SF} at the triple phase contact point.

For contact angles greater than 90°, the surfaces are defined as “hydrophobic”. Most petroleum-derived materials (plastics) are hydrophobic. A higher degree of hydrophobicity can be achieved with polymers where fluorine is substituted for hydrogen (fluorocarbons or fluoropolymers). The C-F bond is unexpectedly covalent and the bond is electronically screened by the large number of fluorine atoms packed along the polymer chain. This gives the fluoropolymer a low surface energy as the surface is homogeneous and non-polar [9]. The C-F bond is also non-reactive, which is critical for preventing oxidation or reduction of the fluoropolymer during electrowetting. Fluoropolymers typically have water contact angles in the range of ~110-120°. Surfaces with contact angles larger than 150° are termed as “super hydrophobic”. Super hydrophobic surfaces are almost always achieved through surface texturing and incomplete droplet wetting, commonly referred to as the Cassie-Baxter state [10]. “Hydrophilic” surfaces such as inorganic glasses have contact angle less than 90°, while “super hydrophilic” surfaces have contact angles smaller than 10°. Hydrophobic surfaces imply that the intermolecular forces inside the water droplet are much stronger than the forces between the molecules of water and the surface. The converse for the hydrophilic surfaces is true.

In electrowetting, it is desirable to have a large initial contact angle in order to maximize the change in contact angle that can be achieved as voltage is applied. Hence, a fluoropolymer with a low surface energy (γ_{AF}< 16 mN/m) is used as the top surface throughout this thesis. Throughout this thesis, the de-ionized (DI) water droplet has a high surface tension of γ_{SA}~73mN/m.

2.1.2 Contact angle on a rough surface

The contact angle of a water droplet on a random rough surface is highly dependent on the surface roughness. The macroscopic contact angle of water droplet on a random hydrophobic surface (θ_c) is different from the contact angle of a water droplet on a planar surface (θ_o). A closer look at the random surface reveals many air gaps as shown in fig. 2.2.

The macroscopic contact angle is obtained by averaging the interfacial surface tensions γ_{SA}(water/air) and γ_{SF} (water/fluoropolymer) between the water and the rough surface. This effect is theoretically represented by the well-known Cassie Baxter equation:

$$\cos\theta_c = f\,(\cos\theta_o + 1) - 1 \qquad 0<f<1 \qquad (2).$$

Where, f is the fraction of solid material contact with the liquid and 1-f being the remainder of the liquid/air contacts between the areas of liquid/solid contact [11]. In simplest terms, air has essentially zero surface energy. Therefore as the roughness increases, the droplet is supported by more pockets of air and less solid material. As roughness continues to increase the system approaches that of a droplet in air (a perfect sphere) and hence the super hydrophobic effect arises.

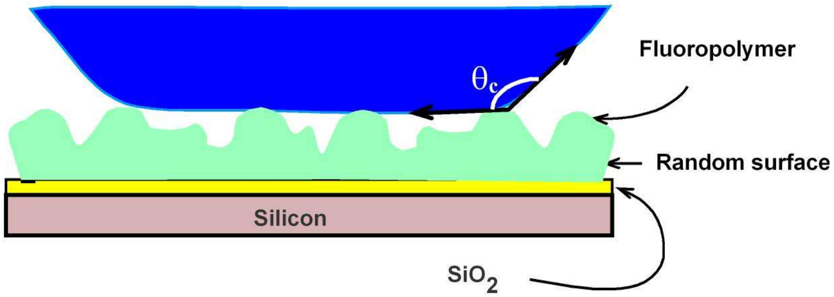

Fig 2.2, Contact angle θ_c of the water droplet on a random hydrophobic surface.

2.2 Electrowetting

2.2.1 Electrowetting on a planar surface

Electrowetting occurs when water is electrostatically attracted to the surface underneath. This is governed by the Young's-Lippmann equation (3)

$$\cos\theta_V = \cos\theta_O + \frac{\varepsilon_o \varepsilon_r}{2\ z\ \gamma_{SA}} V^2 \qquad (3)$$

The electrowetting angle θ_V depends on the initial contact angle θ_o and an electrostatic term. This electrostatic term is proportional to the voltage V applied, relative dielectric constant of the fluoropolymer ε_r or k; inversely proportional to the thickness of the fluoropolymer z and water/air interfacial surface tension γ_{SA}. Fig. 2.3(b) shows a water droplet being electrostatically attracted to the insulator (dielectric) underneath it. When no voltage is applied across the droplet, the droplet is present in its hydrophobic state as in fig. 2.3(a).

It should be noted that throughout this thesis, for simplicity electrowetting is explained as an electromechanical or electrostatic effect.

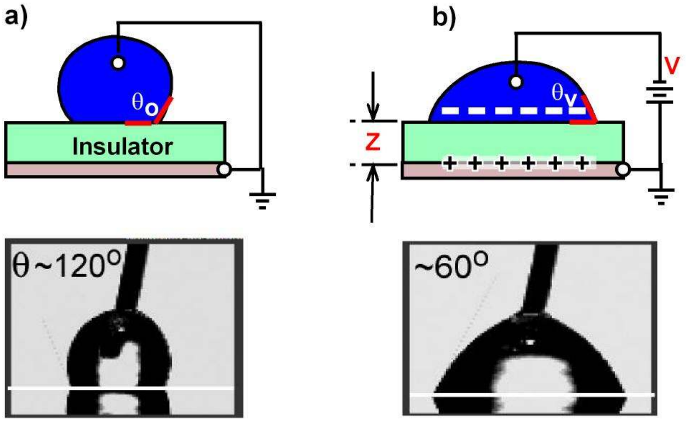

Fig 2.3, (a) Water droplet present on a hydrophobic insulator without applied potential. (b) Under voltage bias V, the water droplet is electrostatically attracted to the insulating dielectric underneath.

The thermodynamic explanation of electrowetting deals with reduction of interfacial surface tension with increased surface charge (the Lippman effect). However, the conclusions in this thesis are not dependent on details beyond the electrowetting equation and Lippman behavior need not be analyzed in detail.

In electrowetting, usually a negative bias is applied to the water droplet, as it is observed that application of positive voltage bias increases the probability for electrolysis of water. Fig. 2.4 depicts the usual electrowetting structure in which, the dielectric is sandwiched between water droplet and the silicon substrate, this device structure is equivalent to a capacitor with the capacitance dependent on the thickness and dielectric constant of the dielectric. With voltage bias as in fig. 2.3(b), charge accumulation takes place near the water-dielectric interface as in fig. 2.4. The charge accumulated is proportional to the voltage applied and the capacitance per unit area of the dielectric. The charges accumulated on the water side of the water-fluoropolymer interface results in an electrowetting force F_{EW} which can then be summed with the in-plane interfacial surface tension forces.

F_{EW} is proportional to the charge per unit area accumulated at the water/dielectric interface. This force F_{EW} counters the interfacial water/fluoropolymer surface tension.

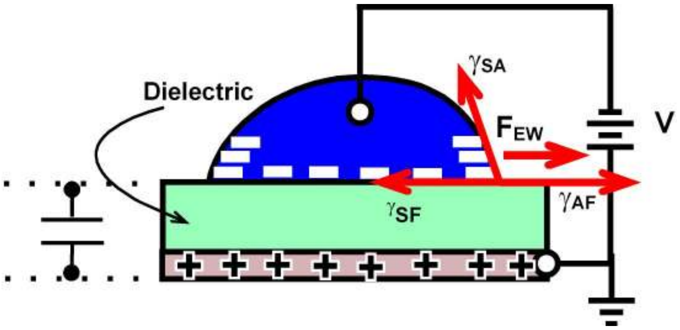

Fig 2.4, Diagram of electrostatic attraction of droplet to the surface of dielectric.

As a result, the modified equivalent interfacial water/air surface tension can be written as

$$(\gamma_{SF})_{new} = \gamma_{SF} - F_{EW} \qquad (4)$$

eqn. 1 and $(\gamma_{SF})_{new} < \gamma_{SF}$, it is obvious that the corresponding new contact angle θ_V is less than θ_o. Hence, the water droplet wets the surface.

2.2.2 Contact angle saturation

When the voltage bias applied to water droplet is increased to an extent such that $F_{EW} = \gamma_{SF}$, the net interfacial water/fluoropolymer surface tension, i.e. $\gamma_{SF} - F_{EW}$ becomes zero. This is the thermodynamic electrowetting limit of the droplet. The contact angle at thermodynamic electrowetting limit can be obtained from eqn. 1 and using that $\gamma_{SF} = 0$;[12]. The contact angle at thermodynamic electrowetting limit is given by

$$\theta_v = \cos^{-1} (\gamma_{AF} / \gamma_{SA}) \qquad (5)$$

Electrowetting does not extend beyond this limit for thermal equilibrium (gradual application of DC voltage). Typical electrowetted contact angles for the limited case are ~70-90° for most electrowetting materials systems. The charges continue to accumulate beyond the electrowetting limit, but they do not contribute to further wetting. As mentioned, this only applies to gradual application or ramping of DC voltage. Any detraction from this bias scheme such as abrupt DC, or AC, takes the system out of equilibrium and therefore the electrowetting limit no longer applies.

For abrupt AC or abrupt DC the electrowetted contact angle can exceed the electrowetting limit by several 10's of degrees (~70-30° for various materials systems). For this case beyond the electrowetting limit, the point at which contact angle reduction becomes once again limited is referred to as electrowetting saturation. At this voltage, the most often mechanism causing saturation is charge injection into the hydrophobic

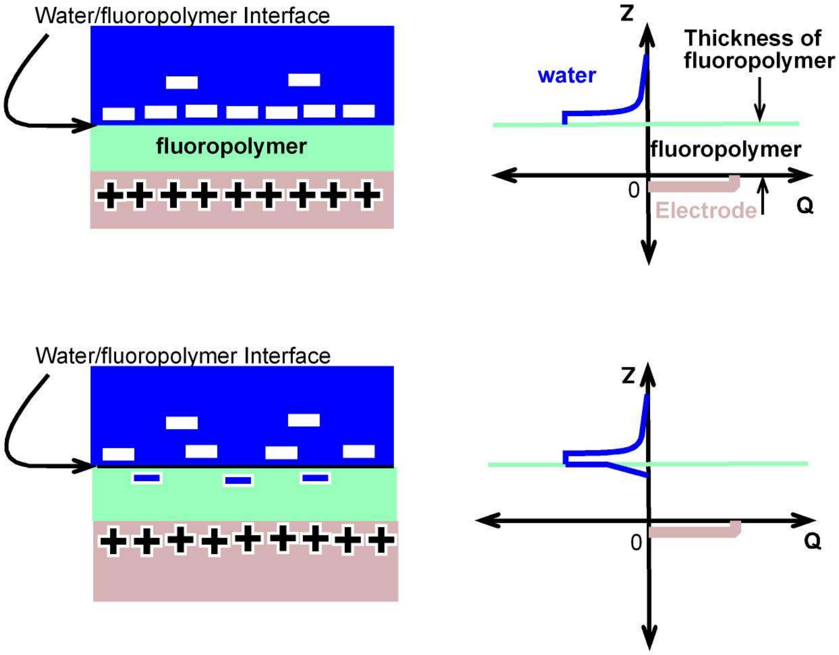

Fig 2.5, (a) Water/dielectric interface before contact angle saturation. (b) Accumulated and injected charges after contact angle saturation.

dielectric as in fig. 2.5(b). These injected charges mask the effect of increased positive charges on the dielectric side at the interface. Therefore, there is a little or no increase in the F_{EW} force after the saturation limit. As a result, the contact angle of water does not change after saturation even though higher voltages are applied [13].

In fig. 2.5(b) z denotes the spread distance of charges from the interface. With application of even higher voltages beyond saturation voltage, the charges injected into the dielectric exceedingly mask the field of charges accumulated on water side of interface causing the droplet to rise back slowly. It is preferred to operate the electrowetting device well away from saturation as electrowetting behavior is much less predictable near saturation.

2.3 Low-voltage electrowetting

It is easily understood that one would desire to operate electrowetting devices at low voltages. This would have a great impact on electrowetting device applications in e-paper, lab-on chip devices and displays. The conditions for low-voltage electrowetting can be obtained from eqn. 3. These are as follows:

- Decrease z i.e. thickness of dielectric.
- Decrease γ_{SA} i.e. interfacial surface tension between water and the surrounding ambient.
- Increase k of the dielectric used.

2.3.1 Single-liquid electrowetting

The decreased thickness approach has been the common approach to achieve lower-voltage electrowetting. This is often implemented by decreasing the thickness of the hydrophobic layer formed on top of a thick high-k dielectric layer. This dielectric stack is shown in fig. 2.6. In this stack, the thickness of high-k dielectric is z_k and thickness of hydrophobic dielectric is z_F. These dielectrics have capacitances C_k (high-K dielectric) and C_F (fluoropolymer) in series, which result in an equivalent capacitance dominated by the lower valued capacitance.

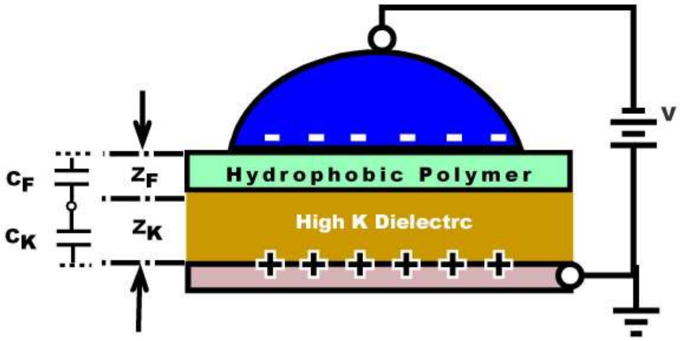

Fig 2.6, Diagram of electrowetting on a dielectric stack.

So to increase the capacitance of the fluoropolymer, the thickness of the fluoropolymer is decreased in accordance with eqn. 6.

$$C = \frac{A\varepsilon_o K}{Z} \qquad (6)$$

There are certain disadvantages associated with this approach, which hinder the full potential of increased capacitance. The presence of the high-k dielectric underneath the fluoropolymer to prevent dielectric breakdown is only marginally effective. The charge tends to inject through the fluoropolymer and accumulate at the fluoropolymer/high-k dielectric interface. This causes charge screening and therefore electrowetting saturation as explained in the previous section.

2.3.2 Two-liquid electrowetting

To reduce γ_{SA}, it is necessary to add surfactant to the water or to change the environment around the water droplet (the air). The environment can be changed by replacing air with oils like dodecane. Interfacial surface tension of water/oil is less than the interfacial water/air surface tension (~30-50 mN/m compared to ~73 mN/m, respectively). According to eqn. 3, reducing interfacial surface tension reduces the operating voltage. This approach can be further beneficial if the oil is density matched to the water droplet. This reduces the effect of vibration or gravity on the system. It is observed that the water droplet surrounded by oil takes longer duration to rise back to its initial state when the voltage is removed than when it is surrounded by air. This is due to the reduced water/oil surface tension, i.e. less restoring force to pull back the water droplet back up after the voltage is removed. Electrowetting speed can also be reduced due to the increased viscosity of the surrounding environment. Reduced speed therefore places a limit on this approach (i.e. surface tension cannot approach zero). Therefore alternate means of decreasing operating voltage are still needed.

2.3.3 Increasing dielectric constant k

Conventional fluoropolymers or other smooth hydrophobic materials that have a large initial contact angle have a small dielectric constant (k <4). On the other hand, high-k dielectrics are not hydrophobic. High-k dielectrics have strong polar domains resulting in a high surface energy and wetting by polar liquids such as water. Therefore, high-k dielectrics are not available for use in electrowetting. Examples of hydrophobic materials with their dielectric constants are listed in tbl. 1.

Therefore, new hydrophobic materials, with increased dielectric constant are required. This thesis proposes that preparing a nanocomposite out of high-k nanopowders and a fluoropolymer can result in proper hydrophobicity and reduced electrowetting voltage.

Table 1, Hydrophobic materials and dielectric constants.

Name	**Dielectric Constant**
Fluoropel, Cytonix Inc.	2
Teflon AF, Dupont Inc.	2
Paraffin	2-2.5
Parylene C	3

CHAPTER 3

SAMPLE PREPARATION & TEST SETUP

3.1 Nanocomposite dielectric preparation

A nanocomposite dielectric was prepared by dispersing high-k barium titanate ($BaTiO_3$) nanopowder (HPB-1000, TPL Inc.) in a fluoropolymer (Fluoropel 1601V, Cytonix Inc.). $BaTiO_3$ nanopowder with spherical morphology and mean particle size of 56 nm is utilized to create a high-permittivity phase within the fluoropolymer (HPB-1000, TPL Inc.). Nanoscale $BaTiO_3$ was chosen because the desired dielectric film thickness is in the range of a micron. If the $BaTiO_3$ particles were micron-size, the film would not function as a fairly homogeneous composite. The SEM of the $BaTiO_3$ nano particles is shown in fig. 3.1

Assuming random orientation for the phase pure cubic $BaTiO_3$, the average dielectric constant can be assumed to be $\varepsilon_r > 300$. The basic idea was to disperse $BaTiO_3$ nanopowder in 1 wt. % fluoropolymer using an ultrasonicator for 30 minutes. This idea resulted in a dispersion which was stable for a short time, with $BaTiO_3$ sediment

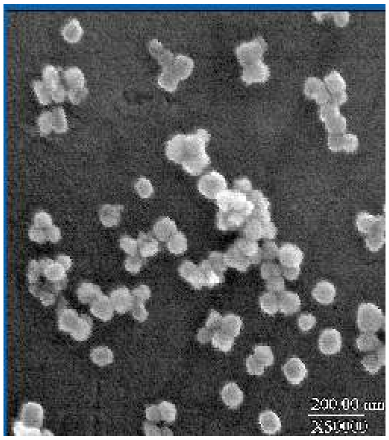

Fig 3.1, SEM of $BaTiO_3$ nanoparticles (Courtesy TPL Inc.).

increasing with time. In order to increase the stability of the dispersion, the nanopowder is dispersed in the fluoropolymer using a silane. Among the different silanes used, fluorosilane ($CF_3 (CF_2)_4 Si (OCH_3)_3$, IT CFB 3958, Dow Corning) is observed to be a good dispersant for the required composite dielectric. This silane is used for preparing all of the composite dielectric samples in this thesis. The suspension of $BaTiO_3$, fluorosilane and fluorosolvent (PFC 1600V, Cytonix Inc.) is ultrasonically treated for 30 minutes. A desired volume of fluoropolymer is then added to the suspension and dissolved. Different samples of composite dielectric are prepared with varying compositions by vol. % of $BaTiO_3$ with respect to the fluoropolymer. This is done to obtain a good comparison among the samples with varying $BaTiO_3$ content.

3.2 Test sample preparation

The test samples are prepared by spin coating the composite dielectric on an oxidized silicon wafer with oxide thickness of 100nm. It should be noted that the oxidized wafer is used only to inhibit electrolysis of water at pores or other defects in the nanocomposite film. The spin parameters for spin coating composite dielectric vary from 1500rpm to 2000rpm for 30 seconds depending on the density of the nanocomposite dielectric. The spin speed was adjusted to keep the film thicknesses constant as much as possible, even though the $BaTiO_3$ content was varied significantly. The samples are rested for 2 hours to allow the films to cure slowly and achieve the maximum possible surface flatness. This slow cure also increases the density of the film for the case of very high $BaTiO_3$ loading. Samples are then baked in the oven at 120°C for 30 minutes. The samples obtained have a characteristic roughness arising from the $BaTiO_3$ particles present near the surface of

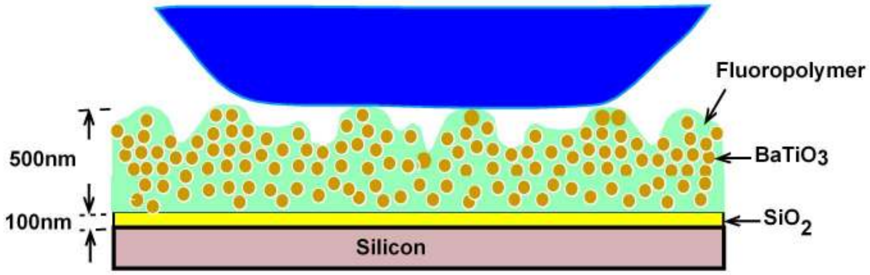

Fig 3.2, Nanocomposite dielectric layer diagram.

the dried film. The film morphology with $BaTiO_3$ nanoparticles is depicted in fig. 3.2

Roughness of the film to a high degree is not advantageous to electrowetting. As it is observed that it would lead to very strong wetting hysteresis. The morphology of the samples is confirmed by AFM scans of 50 vol. % $BaTiO_3$. The AFM scan of 50 vol. % $BaTiO_3$ without the top coat is shown in fig. 3.3

To reduce surface roughness, the samples are dip-coated in the 1% fluoropolymer. The dip coat draw speed is calibrated to get a 500 nm thick dried fluoropolymer film on top of a smooth surface. Some samples had little or no surface roughness i.e. with $BaTiO_3$ composition < 25 vol. % and a 400nm thick top coat. Samples with moderate surface roughness had $BaTiO_3$ composition < 75 vol. % and a 300nm thick top coat, while samples with a very high surface roughness exceeding 75 vol. % in $BaTiO_3$ composition

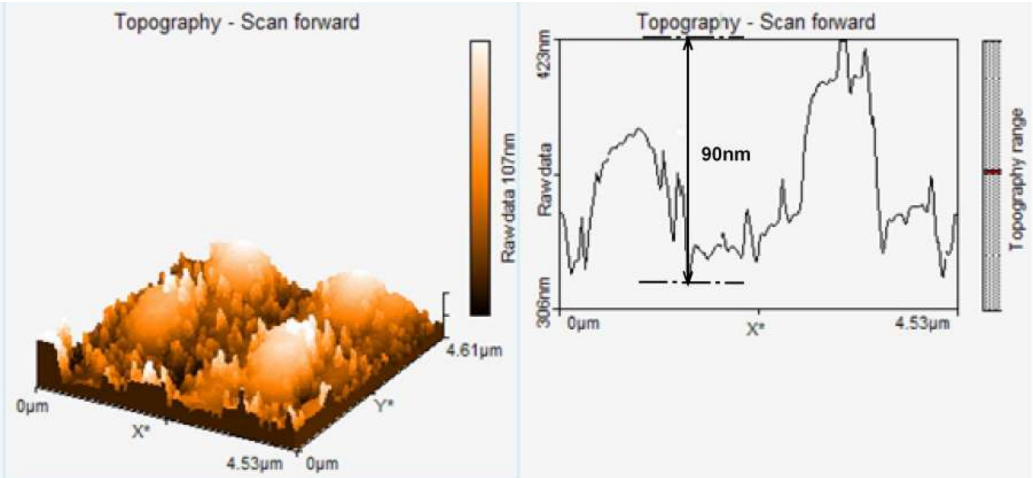

Fig 3.3, AFM scan of 50 (vol. % of $BaTiO_3$) without the top coat.

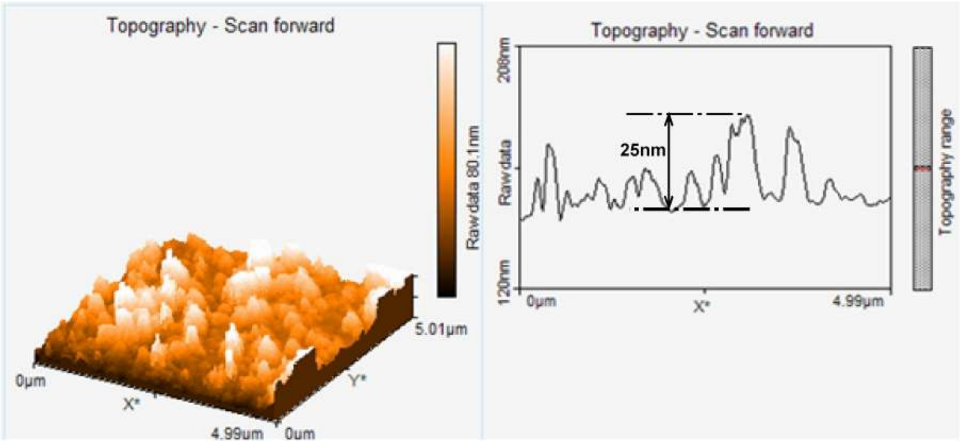

Fig 3.4, AFM scan of 50 (vol. % of $BaTiO_3$) after the top coat.

had less than 100nm thick top coat of fluoropolymer. These values are confirmed by the AFM scans taken after the top coat of fluoropolymer as in fig. 3.4.

It is believed that increasing $BaTiO_3$ results in increased film porosity, and therefore additional fluoropolymer coating fills any pores between $BaTiO_3$ particles before adding to the thickness of the film stack. This layered structure was utilized in all electrical testing and is shown in fig. 3.5.

In practice, it would not be necessary to do a top coat for all the composite dielectric samples. For example, the top coat is not necessary for samples with low $BaTiO_3$ content. The top coat is only needed for samples with high $BaTiO_3$ content. However, to achieve

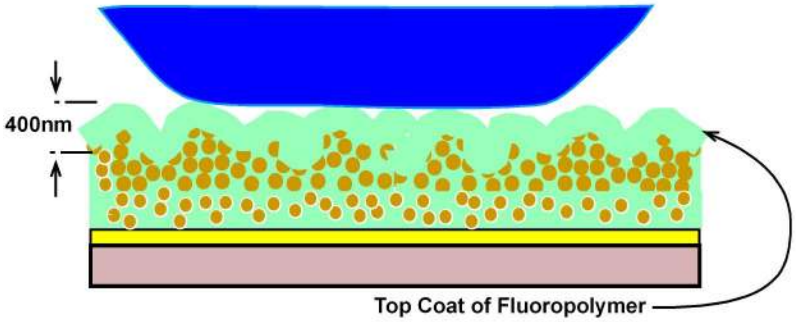

Fig 3.5, Composite dielectric structure after the fluoropolymer top coat.

effective comparisons for the experiments performed herein, a top coat of pure fluoropolymer was done on top of all composite dielectric films.

The thickness of the film stack (composite fluoropolymer/fluoropolymer) is measured using a Dektak profilometer. The dip coating parameters and spin parameters of the samples with various $BaTiO_3$ compositions were adjusted to achieve a final film thickness ranging from 0.8 µm for the pure fluoropolymer to ~1.2 µm for the films with primarily $BaTiO_3$ content. This film thickness variation was accounted for in the experimental data and related theoretical calculations.

3.3 Test setup

Three setups are used to characterize the composite dielectric films.

1. Capacitance.
2. Contact angle vs. voltage measurement.
3. Charge -voltage (Q-V) analysis.

Test voltages were provided by the combination of an arbitrary function generator (AFG310, SONY Tektronix) and a linear voltage amplifier (F20ADI, FLC Electronics). The function generator provides many types of voltage source functions which include sinusoidal, square, pulse, DC etc. In characterizations to be discussed, DC and the sinusoidal are the most used functions. The function generator can provide up to a maximum of 8V output (peak-peak DC level). This maximum output of the function generator is not sufficient to drive the electrowetting devices. So, a linear voltage amplifier (F20ADI) with voltage amplification of 20X is used in series with the function generator to account for a maximum of 160V that is used for characterization. Together the combination met the needs posed by the various experiments.

3.3.1 Capacitance

On the test samples, a small test area is achieved with a small square with typical dimensions 2.5mm X 2.5mm. The boundary of the square is lined with polyimide (Kapton, Dupont Inc.) of thickness 25um. The Kapton thickness is much greater than the thickness of the fluoropolymer/composite dielectric. Therefore, the measured capacitance area is fixed and is only that confined within the 2.5x2.5 mm region. If this approach were not implemented, the droplet contact area is not known. A saline solution (1% KCl solution) droplet is confined within the boundaries of the square such that it covers the entire exposed composite dielectric stack film. This is used as one end of the probe for capacitance measurement and the other probe being the silicon substrate. The surface of the composite dielectric film and silicon dioxide is scribed to expose silicon. The electrical contact to the silicon substrate is made by using silver paste and a copper wire. The capacitances of films were taken before and after the top coat over the composite dielectric. The capacitance characterization setup is shown in fig. 3.6.

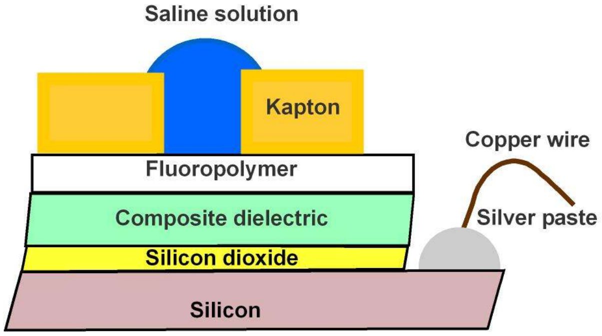

Fig 3.6, Capacitance characterization setup.

3.3.2 Contact angle vs. voltage measurement

The contact angle of the film is measured using the VCA optima contact angle measurement system. Contact angle measurements (θ_v) are taken with negative DC bias applied to the De-Ionized (DI) water droplet, with the silicon substrate as ground. Unlike the capacitance measurements, not Kapton tape boundary is utilized. The voltage is decreased in steps of 4V per second from 0 to -160V. A picture is taken on the VCA optima workstation using dynamic capture with a frame taken every second corresponding to each voltage step. The contact angles of the water droplets in all the 40 frames is measured and is exported to SPC format file using VCA optima contact angle software. The file is then imported onto MS Excel and KaleidaGraph 4.0 data file. A graph is plotted with contact angle at every voltage using MS Excel data file. The contact angle vs. voltage data set is taken for each test sample before and after the top coat.

3.3.3 Charge-voltage (Q-V) analysis

The Q-V analysis is done using a setup developed by Wager [14] for characterization of inorganic thin-film-electroluminescent devices. This thesis is the first report of this technique applied to electrowetting. The Q-V analysis setup consists of a series combination of a resistor, device under test and a sense capacitor. The sense capacitance is usually 100 times greater than that of device under test, so that most of the applied voltage occurs across the device. This series combination is driven by a waveform generator. For the circuit used, a sinusoidal voltage with peak to peak voltage varying from 0 to 160V at a frequency of 1 Khz is applied to the sample as shown in fig. 3.7.

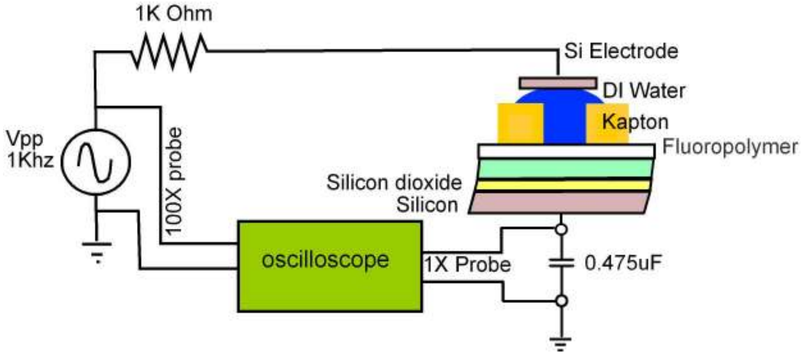

Fig 3.7, Q-V setup using sensing capacitance method.

A DI water droplet is sandwiched between a silicon electrode and the sample, pinned within a specific region of known area lined by polyimide (Kapton). A 1X probe is connected across the sensing capacitance to the channel 2 of an oscilloscope. The oscilloscope can measure up to a maximum of 40V. So, a 100X probe is connected across the voltage supply to the channel 1 of the oscilloscope. The oscilloscope is operated in XY mode, with Channel-1 on X-axis and Channel-2 represented by Y-Axis. With this setup, Q-V analysis curves are obtained on the oscilloscope. This data is fed into computer using GPIB connector and using Tektronix software 'Wavestar for oscilloscopes'. Using these curves at backdrop, tracing lines are drawn and formatted in Macromedia Freehand MX. The Y-axis of the obtained graph corresponds to the voltage across the sensing capacitance, while X-axis represents the applied voltage. The scale on Y-axis is converted from voltage to coulombs using an eqn. 7 and the corresponding data points are obtained. In this process of conversion, capacitances within the device affect the charge accumulation. These capacitances of various devices/layers that affect the stored charge in the composite film stack are shown in fig. 3.8.

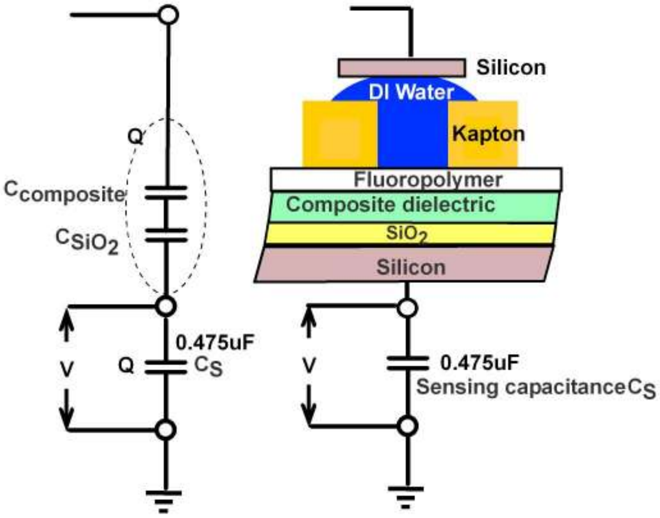

Fig 3.8, Capacitances for Q-V measurement.

Capacitance across the composite dielectric with top coat is given by $C_{composite}$ while the capacitance of the silicon dioxide is C_{SiO2}. The charge $Q_{composite}$ across $C_{composite}$ is given by a simple calculation involving equivalent capacitances and applied voltages.

Thus, the conversion formula is shown in eqn. 7.

$$Q_{composite} = C_s V . \frac{(C_{SiO_2} + C_{composite})}{C_{SiO_2}} \quad (7)$$

Where, C_s being sense capacitance, V being applied voltage.

Test samples with different vol. % compositions of $BaTiO_3$ in the nanocomposite dielectric have been fabricated. They are characterized and tested using the setups mentioned in this chapter. Comparisons are drawn with respect to the pure fluoropolymer. The results are discussed and analyzed in the next chapter.

CHAPTER 4

RESULTS AND ANALYSIS

This chapter contains four sections of results that include:

- Nanocomposite film wetting and electrical properties;
- Electrowetting response for nanocomposite films;
- Bistable wetting behavior;
- Charge-voltage analysis;

At the end of this chapter, preliminary discussion is included on the nature of charge trapping in the nanocomposite films.

4.1 Nanocomposite film wetting characteristics and properties

Hydrophobic dielectrics are used in electrowetting such that the water droplet attains a large initial contact angle. This provides a greater change of contact angle with applied voltage than the case of electrowetting on hydrophilic surfaces. Test samples with varying $BaTiO_3$ vol. % compositions retain this much needed hydrophobicity of the fluoropolymer. This is confirmed by contact angle measurements on the sample's surfaces, which reveal larger contact angles compared to contact angle of the pure fluoropolymer without the $BaTiO_3$. This increased contact angle is achieved with change in surface roughness of the fluoropolymer by presence of $BaTiO_3$ nanopowder. The unique ability of our nanocomposite dielectric to manipulate initial (zero bias) contact angle by controlling random surface roughness is an additional advantage/achievement for the nanocomposite approach. The contact angle change for rough surfaces can be estimated by Cassie Baxter factor *f* given by eqn. 2. This change of contact angle by random surface roughness is described in [11]. The increased contact angle in case of nanocomposite dielectric can be estimated by *f*. For this work, *f* can be theoretically related to the volume fraction of $BaTiO_3$ in fluoropolymer given by

$$f \sim (1- \text{ vol. fraction of } BaTiO_3)^{2/3} \qquad (8)$$

f [11] represents the fraction of original material present on the surface. From this definition, a simple approximation can be made assuming a cube of nanocomposite dielectric having x volume fraction of $BaTiO_3$. The volume fraction of fluoropolymer in that cube is 1-x. A side of the cube would have a $(1-x)^{2/3}$ surface distribution of fluoropolymer. The top of the film would therefore track the relationship provided in eqn. 8.

According to the data presented in tbl. 2, the slope of *f* vs. vol. % $BaTiO_3$ is in fair agreement between measured and approximate theoretical value (eqn. 8). The slight discrepancy in measured vs. theoretical values in this work could be due to the settling time (slow cure at room-temp) that allows the $BaTiO_3$ nanopowder to pack more tightly in the cured film. This would result in increased amount of fluoropolymer on the surface compared to $BaTiO_3$. The samples with $BaTiO_3$ > 50 vol. % have surface roughness to the point where contact angle increases, as mentioned in section 3.1 the pure fluoropolymer top coat can smooth the surface roughness. This decrease in surface roughness by top coat of fluoropolymer is directly evidenced in tbl. 2 as a reduction in liquid contact angle.

Table 2, Comparison of contact angle at zero bias before and after final dip coating in fluoropolymer 1.

Vol. % of $BaTiO_3$ in composite dielectric	Contact angle θ_c of composite dielectric before fluoropolymer top coat	Contact angle θ_c of composite dielectric after fluoropolymer top coat
0	104	104
20	106.2	104
50	108.5	105.2
66	109.5	106.7
75	120	111
97	133	121.7

In the above data set, it was suspected that significant silane contamination of the fluoropolymer surface was occurring. The silane contamination occurred during top coat processing of numerous samples. This contamination was reducing the initial contact angle below the theoretically expected value of ~115-120°. Therefore a fresh fluoropolymer solution was implemented, and used for a smaller sample set to reduce contamination. This new data set, shown in tbl. 3 exhibited behavior more in line with theoretically expected results.

Two important conclusions for these tests are summarized:

- Increased $BaTiO_3$ content leads to increased film roughness and thereby a large initial contact angle.
- The fluoropolymer top coat performs its intended function of smoothing the dielectric top surface, as witnessed by a reduction in contact angle.

Table 3, Contact angle with fluoropolymer 2.

Vol. % of $BaTiO_3$ in composite dielectric	Contact angle θ_c of composite dielectric before fluoropolymer top coat	Contact angle θ_c of composite dielectric after with fluoropolymer top coat
0	117.8	117.8
50	118.6	118.5
75	123.25	119

4.1.1 Optical properties

Table 4, Diffuse reflectivity %.

Vol. % of $BaTiO_3$	Diffuse reflectivity %
0	1.6
50	6
75	6.9
75 (without top coat)	13

With the integration of $BaTiO_3$ nanoparticles, the nanocomposite dielectric films exhibited diffuse reflectivity. The diffuse reflectivity % of various samples with top coat is shown in tbl. 4. Since electrowetting devices are often used for optics, this is an important measurement to provide. In some cases, such as reflective electrowetting displays increased diffused reflectivity is desired [4].

4.1.2 Electrical properties

The electrowetting properties of a hydrophobic dielectric are best analyzed using contact angle (θ_v) vs. voltage (V) characterization. This contact angle vs. voltage is theoretically predicted by the Lippmann-Young's eqn. 3. Of interest to this thesis is that this equation can reveal factors that lead to lower-voltage electrowetting. One route for achieving lower-voltage electrowetting is to increase the dielectric capacitance. The capacitance per unit area of the samples is found using the capacitive setup discussed in 3.3.1 and a capacitance meter. The capacitances of different layers are found before and after top coat of fluoropolymer. The capacitances of different layers of the composite dielectric (with top coat) are shown in fig. 4.1.

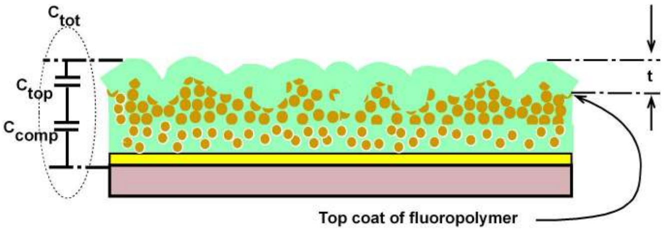

Fig 4.1, Capacitances of different layers on the composite dielectric stack.

C_{comp} represents the capacitance of the composite dielectric layer taken using capacitance setup before the top coat; C_{tot} is the capacitance of the nanocomposite dielectric taken using capacitance setup after the top coat. C_{top} is calculated from C_{comp} and C_{tot}. Knowing C_{top}, one can then calculate the approximate thickness of the fluoropolymer top coat for each sample. The capacitances values of test samples and estimated thicknesses of the top coat are shown in tbl. 5. Observations show that the capacitances of the composite dielectric samples increase with increase in $BaTiO_3$ content. Pure $BaTiO_3$ has a dielectric constant of over 300, while fluoropolymer has a dielectric constant of 2. As the content of $BaTiO_3$ in the nanocomposite dielectric increases, the nanocomposite dielectric would have higher dielectric constant. Also, it can be noticed that the capacitances decreases after the top coat.

Table 5, Comparison of capacitances and estimated thicknesses of the nanocomposite dielectrics.

Vol. % of $BaTiO_3$	Capacitance before top coat ($\mu F/m^2$)	Capacitance after top coat ($\mu F/m^2$)	Theoretical estimation of top coat thickness (nm)
0	38.42	14.7	400
20	38.42	14.9	400
50	153.3	33.3	224
66	217.39	39.	200
75	410.11	51.6	161
97	1510.5	82.3	109

The reason could be explained by assuming a low-k dielectric (fluoropolymer, top coat) in series with a high-k dielectric (composite dielectric, spin coat), which would result in a total capacitance that is limited by the low-k dielectric. Even though the capacitance after the top coat decreases, the capacitance is still greater than that of the fluoropolymer with the same thickness as the composite/top-coat stack. For 50-75 vol. %, a 2-3X increase in total capacitance is achieved with respect to pure fluoropolymer. As will be shown later, this increase of capacitance will reduce the voltage required for electrowetting.

As shown in tbl. 5, the capacitance data can also be used to reveal the thickness of the top coat of pure fluoropolymer. The top coat of fluoropolymer deposited by dip coat on a flat and non-porous surface would result in 400nm thickness after a bake. But, the calculation for the top coat in tbl. 5 reveals that the samples with increased $BaTiO_3$ have reduced fluoropolymer top coat thickness (<400nm). C_{top} is calculated from C_{comp} and C_{tot}. Dielectric constant of fluoropolymer (k ~ 2) is used to calculate the thickness z of the top coat using the eqn. 6. This confirms that the composite dielectrics with higher $BaTiO_3$ content have increased porosity for the underlying composite film. This increased porosity causes the fluoropolymer top coat to sink into the pores and reduce the thickness of pure fluoropolymer residing on top of the composite.

The increasing capacitance observed in tbl. 5 arises with increase in $BaTiO_3$ content arising from increase in the average (bulk) dielectric constant of the stack. To justify this assumption, averaged dielectric constants for the nanocomposite films plus top coat are also calculated and are provided in tbl. 6. Since this is an averaged dielectric constant for the composite + top coat layers, the dielectric constant of the stand-alone composite should be higher. The value of the dielectric constant for the nanocomposite layer

Table 6, Dielectric constants of standard composite dielectrics

Volume percent of $BaTiO_3$ in composite dielectric	Averaged dielectric constant of the composite dielectric stack after the top coat
0	2
20	2
50	4.5
66	6.1
75	10.5
97	18.6

without the top coat was not calculated as it is believed to be not accurate due to the porous nature of high-$BaTiO_3$ content films, i.e. increased depth and electrical contact area of the liquid to an unknown level.

4.2 Electrowetting response

Electrowetting contact angle vs. voltage is plotted in fig. 4.2 a,b. It is important to note that the spread of the data is partially attributed to limitations of the imaging and contact angle calculation software, and the more pronounced data spread after saturation is expected since the electrowetting mechanism is not stable at higher voltages. Therefore the solid lines drawn through each data set are most representative of the actual electrowetting response prior to saturation. Multiple response curves were obtained for each sample and the results were consistent with those shown in fig. 4.2. As stated previously, nanocomposite dielectric samples with smoother top surfaces (tbl. 1) are better for electrowetting as they have less contact angle hysteresis. Therefore, for electrowetting characterization: (1) the $BaTiO_3$ content is limited to 75 vol. % or less; (2) all samples have a top coat of pure fluoropolymer.

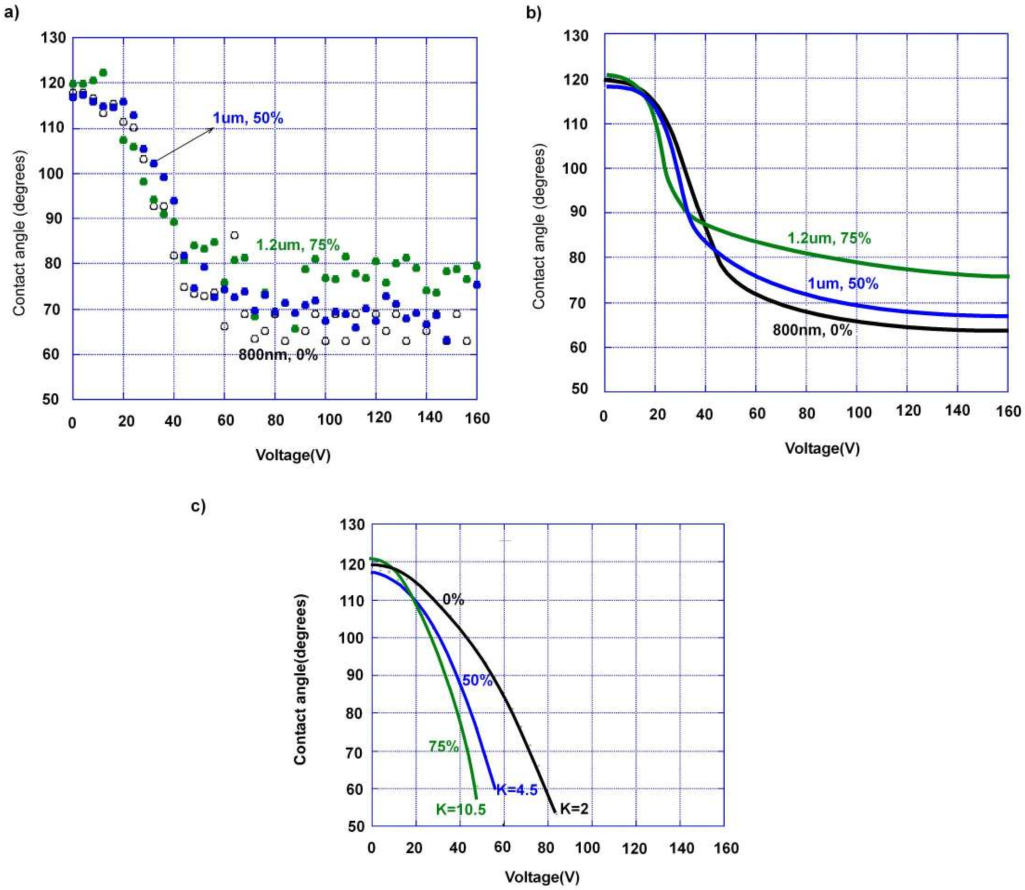

Fig 4.2, Contact angle vs. voltage plots, (a, b) measured and (c) theoretical.

The following conclusions can be made from fig. 4.2:

- Unlike other high-k materials, the nanocomposite dielectrics are able to retain the hydrophobicity of the pure fluoropolymer. This is evidenced by the large contact angle at zero bias.
- *Prior to saturation,* the observed change in the electrowetting response illustrates change in dielectric constant as proved in previous section. As indicated in the plot, the films with $BaTiO_3$ are thicker than the pure fluoropolymer, yet they still exhibit a slightly more rapid electrowetting response over the voltage range of 0-30V. Therefore, according to the

electrowetting equation the only variable that could reduce operating voltage in our experiment is the dielectric constant of the composite dielectric.

Beyond 30V, electrowetting saturation sets in (fig. 4.2c). It is observed from all measurements that increasing $BaTiO_3$ content resulted in early onset of saturation. Saturation limits the ability to continue to decrease contact angle with increasing voltage. Saturation at low voltages with increasing $BaTiO_3$ content is likely due to the charge screening effects discussed in chapter 2. This conclusion will be supported in the next sections that directly measure charge injection into the fluoropolymer.

4.3 Bistability due to charge injection

In addition to reduced operating voltage, this thesis has demonstrated strong-charge storage inside nanocomposite dielectric. This particular property can lead to bistable switching and enhance electrowetting applications in e-paper and lab-on chip devices. For example, bistable switching due to charge trapping would allow an electrowetting display to be switched ON once, and hold it's wetting state without further application of bias. These and other future applications are discussed in the next chapter. First, we will review characterization of charge storage inside the nanocomposite dielectric. It should be noted that we have not optimized the nanocomposite dielectric for maximum or for minimum charge storage. Future work may involve optimization for applications where lower voltage may be desired without charge storage, or applications where very strong charge storage and bistability are desired.

Fig. 4.3 diagrammatically details the charge trapping procedure. Photos of experimental results are shown on the right hand side of fig. 4.3. Fig 4.3(a) illustrates the equilibrium state of water droplet on a hydrophobic dielectric with zero-applied voltage. The expected electrowetting behavior is then shown in fig. 4.3(b). If the voltage pulse duration is adequately long (>100 ms), then there is charge injection into the dielectric shown in fig. 4.3(c). These injected charges screen the charge that would otherwise cause electrowetting. Therefore the droplet on the dielectric rises back to a large contact angle (as discussed in 2.2.2). In fig. 4.3(d) the voltage is reset to 0. This presents a 0V potential to the droplet and therefore results in an electrostatic force between the injected charges in the dielectric and the grounded droplet. The droplet then wets the surface as a consequence of charge inversion at the water/dielectric interface. The charge storage and droplet wetting remains for > 60 s, after which the droplet slowly de-wets the

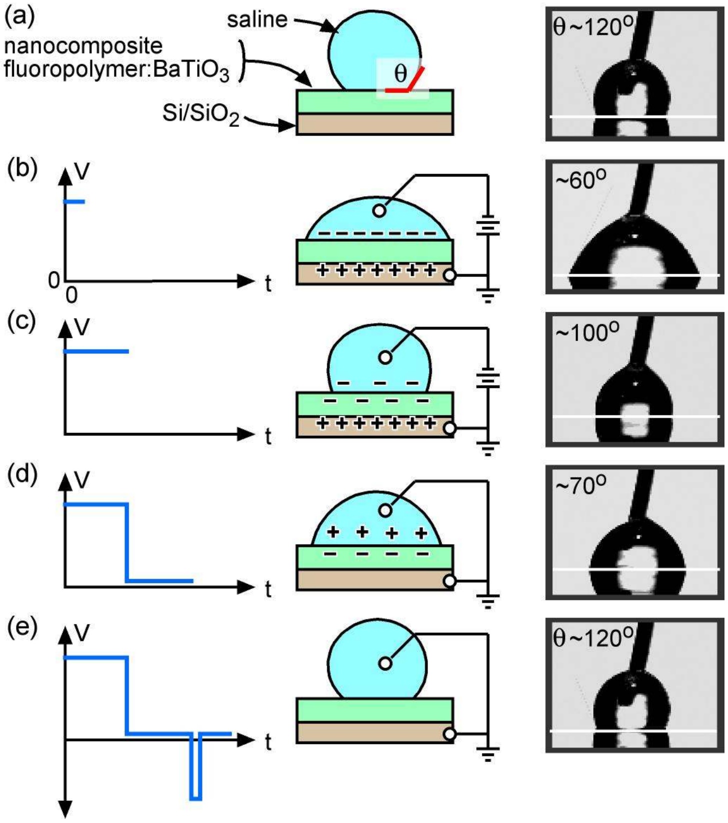

Fig 4.3, Diagrams of contact angle and charge storage.

nanocomposite dielectric and returns to a contact angle > 90°. Strong-charge storage is witnessed for nanocomposite dielectrics with > 75 vol. % $BaTiO_3$.

A particularly powerful feature of the charge-storing dielectric is shown in fig. 4.3(e). When a short positive pulse of 100V (<100 ms) is applied to the water droplet, the composite dielectric discharges majority of the stored charge. Thus, a bistable switching state is demonstrated.

Since the droplet holds it's state for > 60s, without application of external voltage, we refer to this effect shown in fig. 4.3 as bistability. One could argue that bistability should refer to the case where the droplet would hold either wetting state for infinite time. However, for the target applications such as e-paper, this 60s hold time for the droplet fulfills the primary objective of bistability: reduced power consumption. For example, a conventional reflective display is electronically refreshed ~50 times per second. Therefore, the bistable droplet switching reduces power consumption by ~3000X (50x60) compared to conventional electrowetting display technologies. This therefore fulfills the low-power objective of bistable switching.

4.4 Q-V analysis

To further validate that there is charge storage inside the dielectric, various samples were analyzed using the Q-V setup described in the previous section 3.3.3. An ideal (charge-voltage) Q-V curve for device under test would resemble fig. 4.4.

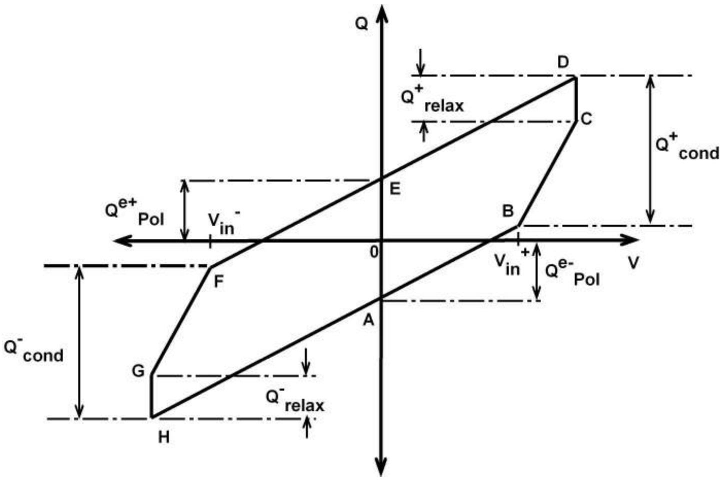

Fig 4.4, Ideal q-v graph with various charges labeled[14].

The presence of superscripts '+' and '-' denote the polarity of the applied voltage. V_{in} denotes applied voltage beyond contact angle saturation due to the onset of charge injection. Q_{cond} is the conduction charge injected into the dielectric beyond contact angle saturation achieved at V_{in}; this is increases the stored charge. Charge storage increases the Q^{e}_{pol} which is the polarization charge stored in the dielectric at the $BaTiO_3$/fluoropolymer interface just prior to the onset of the subsequent pulse of opposite polarity. Finally, Q_{relax} is the additional relaxation charge that flows into dielectric stack during the portion of the waveform at which the applied voltage is held constant at its maximum value.

The Q-V graph is analyzed in a counter clockwise direction (ABCDEFGH). A non-zero value of Q is observed at A because of polarized charge residing in the dielectric, which is left behind by previous pulse of opposite polarity. The AB portion arises from the rising edge of the sinusoidal voltage applied when the magnitude is less than the saturation voltage. BC also occurs during the rising portion of the applied voltage but the voltage is greater than the saturation voltage. During this period charge injection is observed. CD portion of the waveform corresponds to the portion of the waveform in which external voltage is held constant at its maximum amplitude. Section DE is obtained during the falling edge of the waveform. The remainder of the Q-V curve from E to A is similar to the A-E portion except for the applied voltage being of opposite polarity.

Experimental Q-V results are obtained for the test samples with the setup mentioned in section 3.3.3. These results are shown in fig. 4.5. Fig. 4.5 gives the comparison of charge storage in the pure fluoropolymer with different test samples of composite dielectrics with the top coat.

The straight blue dashed line in each plot is the theoretical capacitance response at a sinusoidal frequency of 1 KHz, *without occurrence of charge storage*. The hysteresis in the Q-V plots depicts the deviation from theoretical capacitance and provides direct measure of the magnitude of the charge stored in the dielectric. The plots are closed curves since the voltage cycle is repetitive (alternating, sinusoidal). Fig. 4.5(a) establishes that there is no significant charge storage in fluoropolymer at zero bias. During the positive cycle, a small hysteresis is observed for the pure fluoropolymer at higher voltage which is consistent with the lower-electrical breakdown field (~0.1 MV/cm) of fluoropolymers in response to positive polarity voltage applied to the droplet [15]. This is not well understood and might be due to the dielectric break down of the fluoropolymer/dielectric stack. When the voltage is decreased, the fluoropolymer begins

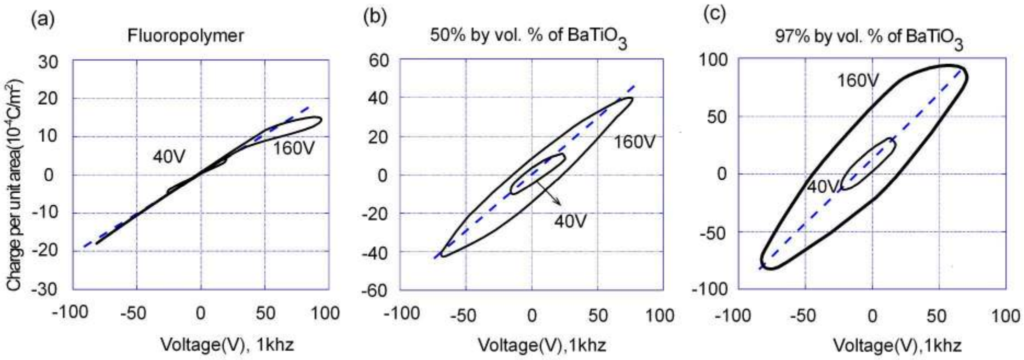

Fig 4.5, Q-V plots of composite dielectrics.

to accumulate charge again and hence a hysteresis is observed. Further not well understood at this time, it is observed for nearly all fluoropolymer films that the breakdown field is higher than 0.1 MV/cm with negative voltage applied to the droplet. This is consistent with the absence of hysteresis in the negative bias regime.

Fig. 4.5(b) & 4.5(c) are plots with 50 and 97 by vol. % of $BaTiO_3$. As expected, these plots exhibit many of the features of the ideal plot of hysteretic Q-V analysis shown in fig. 4.4. As the voltage is increased from 0V (as traversed from A in fig. 4.5), there is substantial charge observed at 0V arising from previous voltage cycle. As voltage is increased, the charge in the nanocomposite dielectric increases in proportion to its capacitance (parallel to the dashed blue line for an ideal capacitor). At the saturation voltage and beyond, charge injection is observed. This increases the amount of charge stored inside the composite dielectric (Q, Y-axis) beyond the theoretical value for an ideal capacitor. As the voltage is decreased the charge stored is decreased proportional to the capacitance. Residual charge is observed at 0V, denoting charge storage at zero bias. The amount of charge stored in each of the bias is approximately the same, only opposite in polarity, exemplified by the symmetry of the plot about Y axis. This observation can be used to switch the bistable behavior of the nanocomposite dielectric. The charge stored in the positive bias can be totally discharged by application of the same voltage in negative bias. These 'discharge voltages' can be determined by the voltages at which the charge returns to zero (i.e. 30-40V for both 4.5(a), 4.5(b)).

The following conclusions can be made from fig. 4.5(b) and 4.5(c)

- The test sample with 97 vol. % $BaTiO_3$ has a greater charge at 0V compared to that of 50 vol. % of $BaTiO_3$.

- The charge increase during the rising edge of the voltage is more proportional to capacitance in case of 50 vol. % of $BaTiO_3$ sample. Charge injection in 97 vol. % $BaTiO_3$ dominates charge increase, which is illustrated by the presence of greater deviation from the blue ideal capacitor line.
- The maximum charge stored at 160V is largest in the 97 vol. % $BaTiO_3$ sample, which is expected due to the effect of increased capacitance and increased charge injection.

4.5 Understanding charge storage

There are many possibilities for the origin of charge storage in these devices. Most of the existing charge traps are likely at the $BaTiO_3$/fluoropolymer interface since (1) the fluoropolymer itself is a poor charge trapper; (2) the $BaTiO_3$ should have breakdown field exceeding 1 MV/cm which precludes charge injection into the $BaTiO_3$. Similar trapping at surface states of $BaTiO_3$ dielectrics has been reported [16]. It is mentioned in [16] about $BaTiO_3$ that "the surface contains many traps and therefore, most of the carriers are probably trapped. From this, we may conclude that a surface electron or hole layer exists that has an enormous surface carrier density and that a fraction of these electrons or holes exists as free carriers." In this nanocomposite dielectric the fluoropolymer is fluorine terminated and non-reactive with the $BaTiO_3$. Therefore there are likely numerous unmatched bonds at the fluoropolymer/dielectric interface. These possible charge traps are depicted qualitatively in fig. 4.6, which depicts the band diagram of $BaTiO_3$/fluoropolymer.

The total number of charge trap states should increase with increasing number of $BaTiO_3$/fluoropolymer interfaces (i.e. increasing $BaTiO_3$ content). Further understanding of the exact nature of the charge storage is beyond the scope of this thesis. Future study involving exact nature of the traps might lead to optimized charge storage and performance of the composite dielectric.

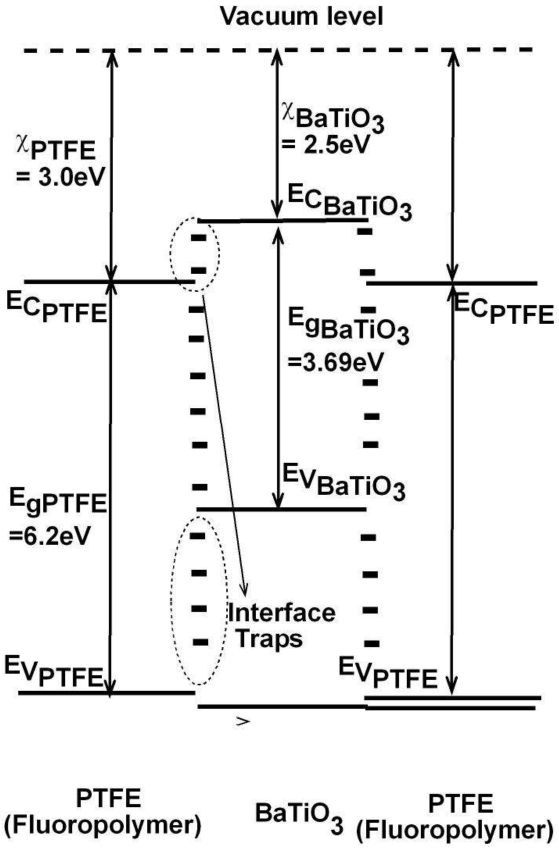

Fig 4.6, Band structure at the interface of $BaTiO_3$ and fluoropolymer with interface traps.

CHAPTER 5

APPLICATIONS

5.1 Electrowetting display

An electrowetting display has been proposed to be brighter and more power efficient than a conventional LCD display [4, 17]. The basic electrowetting display pixel structure and its working are shown in fig. 5.1.

The electrowetting pixel is bounded by a hydrophilic grid. A non-polar dye is used to color the oil. As in fig. 5.1(a), the electrowetting pixel is on, when no voltage is applied. The colored oil spreads on the surface of the fluoropolymer surface giving the entire pixel a red color. The oil spreading is governed by interfacial surface tension forces [4] and occurs for most alkanes such as dodecane. On application of voltage to this device as in fig. 5.1(b), the water encased in the pixel electrowets the fluoropolymer surface and displaces the colored oil to the sides. The water being transparent allows white light to pass through and gets reflected from the reflector underneath the glass substrate. This forms the basic pixel structure of an electrowetting display.

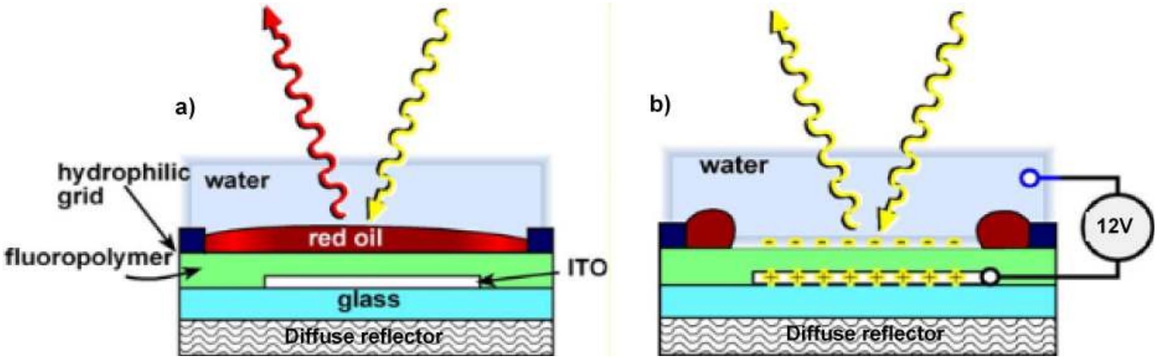

Fig 5.1, Diagram of electrowetting display pixel a) voltage off. b) Voltage on.

5.1.1 Electrowetting transmissive display with composite dielectric

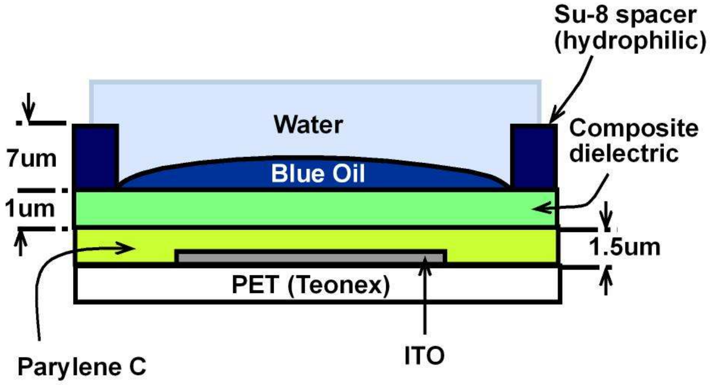

Fig 5.2, Device structure of an electrowetting transmissive display pixel with composite dielectric.

To test the feasibility of the nanocomposite dielectric for electrowetting displays. Display shown in fig. 5.2 was fabricated with 50 vol. % $BaTiO_3$ composite dielectric used in place of the traditional fluoropolymer (fig. 5.1). Also the diffuse reflector present in fig. 5.1 was removed. This allowed light transmissive pixel operation. The transparent substrate was PET (Teonex®, Dupont) with ITO patterned on PET to act as the bottom electrode in the pixel. Parlyene C is used to coat on top of ITO as it is an optically transparent dielectric (k ~3) and it also prevents electrolysis at weak points in the composite dielectric (replacing SiO_2 in the test samples).

In the traditional approach, pure fluoropolymer is used on top of parylene as a hydrophobic layer in the pixel. Typical thickness of the fluoropolymer is 200nm. The fluoropolymer layer is made thin compared to parylene. This lowers the voltage of operation according to section 2.3.1. The operating voltage of the traditional electrowetting pixel is 12V. To eliminate the need of parylene and to lower the voltage of operation, a high-k hydrophobic polymer is needed. This perfectly suits the implementation of the nanocomposite dielectric in place of fluoropolymer. A preliminary

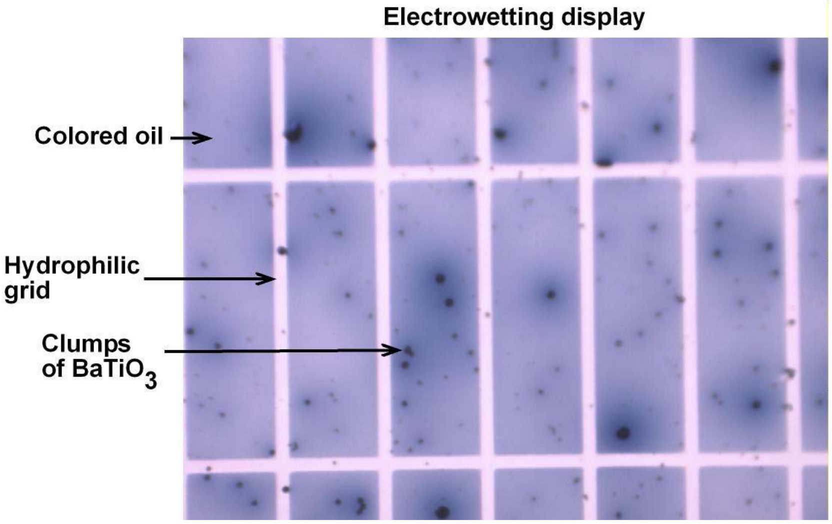

Fig 5.3, Electrowetting display with nanocomposite dielectric.

display device has been fabricated using the nanocomposite dielectric. The device structure is already shown in fig. 5.2. The image of the display pixels with the composite dielectric and blue oil at no external voltage bias is shown in fig. 5.3.

First look at the display reveals clumps of $BaTiO_3$ arising from non-uniform dispersion of $BaTiO_3$ in the nanocomposite dielectric. These clumps are due to the aging of the $BaTiO_3$ dispersion in fluoropolymer prepared earlier to characterize the test samples in chapter 4. These clumps were not present in the devices tested in Chapter 4. This preliminary electrowetting display is analyzed for:

- Low-voltage electrowetting.
- Charge storage (Bistability).

The initial results from the display are very encouraging. The nanocomposite dielectrics with compositions 50 and 75 (vol. % of $BaTiO_3$) are tested. Initial results showed successful lower operating voltage. A comparison of the composite dielectric performance with respect to the use of fluoropolymer in electrowetting display is shown tbl. 7. These preliminary results were not as conclusive as those presented in chapter 4.

Table 7, Nanocomposite dielectric samples and voltages of operation.

Vol. % of $BaTiO_3$	Thickness (nm)	Voltage of operation (V)
0	200	12
50	1000	14
75	1200	10

However it should be noted that the composite dielectric stack thickness is much greater than that of the pure fluoropolymer. Therefore the comparable operating voltage for all three device sets once again confirms that the dielectric constant of the composite is higher than that of the pure fluoropolymer. Due to the need of a smooth surface with the fluoropolymer top coat, the composite films could not be made thinner than the thickness of ~1.0-1.2 μm. This is a good topic for future research in composite dielectrics and would likely call for smaller $BaTiO_3$ particle size.

The voltage response of electrowetting display with 50 vol. % of $BaTiO_3$ is shown in fig. 5.4. An important observation has been made during the switching of the display. The display would not switch back to its previous state when the voltage is removed, i.e. with colored oil spread over the entire pixel area. This is attributed to the high surface roughness arising from non-uniform dispersion of $BaTiO_3$ in fluoropolymer.

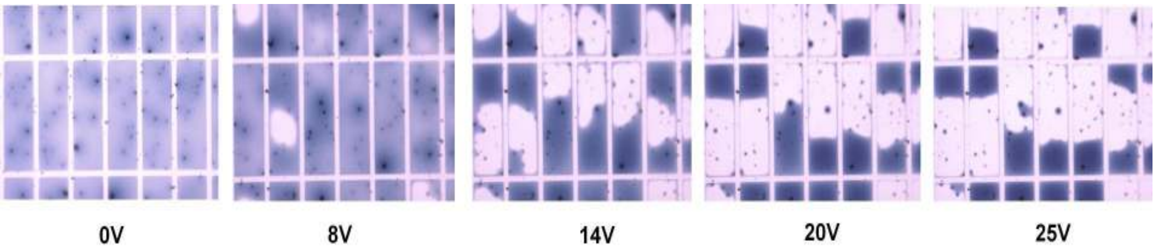

Fig 5.4, Voltage response of electrowetting display.

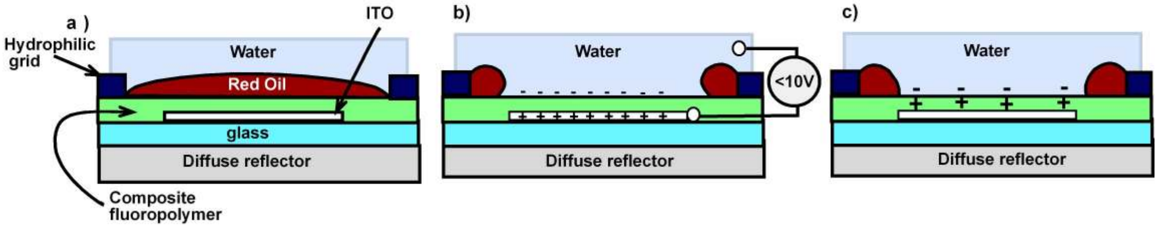

Fig 5.5, a) Device structure with composite dielectric. b) Lower-voltage wetting over fluoropolymer. c) Charge storage and bistable switching behavior.

‘Pinning’ of the oil at $BaTiO_3$ clumps is easily observed in fig. 5.4. This leads to strong hysteresis. Such strong hysteresis was not observed for the samples tested in chapter 4 for two reasons: (1) the fluoropolymer/$BaTiO_3$ solutions were fresher and free from $BaTiO_3$ clumping; (2) the surface tension of water (73 mN/m) is much greater than the oil/water interfacial surface tension used in the display devices (~20 mN/m due to dye acting as a surfactant).

5.1.2 Possible advantages of an electrowetting display with a composite dielectric

If the composite dielectric approach is further developed, replacing the conventional fluoropolymer with the composite dielectric could have many advantages for electrowetting displays.

These include:

a. Lower-voltage operation.
b. Bistable switching (fig. 5.5c).
c. Increased diffuse reflectivity for reflective displays.

In an electrowetting display with conventional fluoropolymer, voltage needs to be applied continuously as long as the state (off) needs to be maintained. For large passive-matrix driven LCD displays [18] the pixels are electronically refreshed ~50 times per second. This leads to power loss even if the image does not change. For emerging applications such as e-paper (i.e. e-book applications) the image does not need to

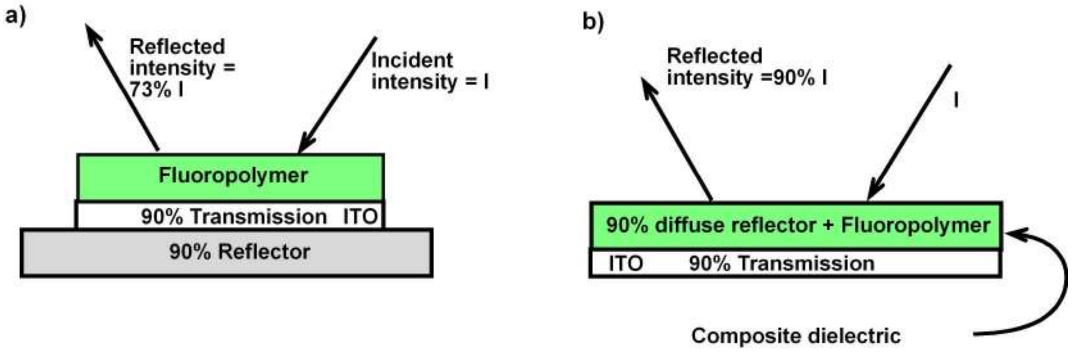

Fig 5.6, Electrowetting display with conventional and composite dielectric reflector layers.

change more than once every several seconds or minutes. Therefore, bistable switching electrowetting dielectrics could reduce power consumption dramatically for such applications and thereby increasing battery life. Other applications that need improved power efficiency include the outer display on clam-shell style cell phones.

Lastly, the diffuse reflectivity of composite dielectric could also be of great importance in improving the brightness of the pixel. This can be shown by fig. 5.6. Fig. 5.6(a) depicts the traditional approach of using a high efficiency reflector behind ITO.

A typical ITO film has a visible spectrum transmission efficiency of 90%. So the intensity of the reflected light is ~ 73% of the incident light intensity as the reflection is 90% (ITO) x 90% (back reflector) x 90% (ITO). Using the composite dielectric in place of the fluoropolymer, the diffuse reflector is incorporated in to the composite dielectric by the presence of $BaTiO_3$; the reflected light intensity with the new layer structure could be as much 90% of the incident light. Given the present results reported in this thesis, smaller $BaTiO_3$ particle size or thicker composite dielectrics are needed to improve the diffuse reflectivity to the point where one could achieve the device in fig. 5.6(b).

REFERENCES

[1] G. Beni and S. Hackwood "Electro-wetting displays," *Appl. Phys. Lett.,* vol. 38, pp. 207-209, 1981.

[2] M. S. Dhindsa, N. R. Smith, J. Heikenfeld, P. D. Rack, J. D. Fowlkes, M. J. Doktycz, A. V. Melechko and M. L. Simpson, "Reversible Electrowetting of Vertically Aligned Superhydrophobic Carbon Nanofibers," *Langmuir,* vol. 22, pp. 9030-9034, 2006.

[3] N.R Smith, D. C. Abeysinghe, J.W.Haus and J. Heikenfeld, "Agile wide-angle beam steering with electrowetting microprisms," *Optics Express,* vol. 14, pp. 6557, 2006.

[4] R. A. Hayes and B. J. Feenstra "Video-speed electronic paper based on electrowetting," *Nature,* vol. 425, pp. 383, 2003.

[5] J. Heikenfeld and A.J Steckl, "Intense switchable fluorescence in light wave coupled electrowetting devices," *Appl. Phys. Lett.,* vol. 86, pp. 011105, 2005.

[6] Perepelkin, "Fluoropolymer Fibres: Physicochemical Nature and Structural Dependence of their Unique Properties, Fabrication, and Use. A Review," *Fibre Chemistry,* vol. 36, pp. 43, 2004.

[7] H. Moon, S.K. Chow, R.L Garrell and C. J. Kim, "Low voltage electrowetting-on-dielectric," *J. Appl. Phys.,* vol. 92, pp. 4080, 2002.

[8] B. Janocha, H. Bauser, C. Oehr, H. Brunner and W. Gopel, "Competitive Electrowetting of Polymer Surfaces by Water and Decane," *Langmuir,* vol. 16, pp. 3349-3354, 2000.

[9] R. Kasowski, W.Y. Hsu and E.B Caruthers, "Electronic properties of polyacetylene, polyethylene, and polytetrafluoroethylene," *J. Chem. Phys.,* vol. 72, pp. 4896-4900, 1980.

[10] K. Krupenkin, J.A. Taylor, T.M Scheneider and Shu Yang, "From Rolling Ball to Complete Wetting: The Dynamic Tuning of Liquids on Nanostructured Surfaces," *Langmuir,* vol. 20, pp. 3824, 2004.

[11] Torkkeli, "Droplet Microfluidics on a Planar Surface," *Technical Research Centre of Finland Publications,* pp. 3, 2003.

[12] Q. Quinn, R.Sedev and J. Ralston, "Contact Angle Saturation in Electrowetting," *J Phys Chem B,* vol. 109, pp. 6268, 2005.

[13] H. Verheijen and M.W.J Prins "Reversible Electrowetting and Trapping of Charge: Model and Experiments," *Langmuir,* vol. 15, pp. 6616-6620, 1999.

[14] F. Wager J and P.D Keir, "ELECTRICAL CHARACTERIZATION OF THIN-FILM ELECTROLUMINESCENT DEVICES," *Annual Review of Materials Science,* vol. 27, pp. 223, 1997.

[15] K. Elanseralathan, M. Joy Thomas and G.R Nagabhushana , "Breakdown of Solid Insulating Materials Under High Frequency High Voltage Stress," *- Properties and Applications of Dielectric Materials, 2000. Proceedings of the 6th International Conference on,* pp. - 999, 2000.

[16] Y. Watanabe, M.Okano and A. Masuda, "Surface Conduction on Insulating BaTiO3 Crystal Suggesting an Intrinsic Surface Electron Layer," *Phys. Rev. Lett.,* vol. 86, pp. 332-335, 2001.

[17] J. Heikenfeld and A.J Steckl, "High-transmission electrowetting light valves," *Appl. Phys. Lett.,* vol. 86, pp. 151121-151121-3, 2005.

[18] G. Lombardo, M. Manuela, B. Riccardo and R.C John"32-channel arbitrary waveform generator for bistable nematic devices," *Rev. Sci. Instrum.,* vol. 75, pp. 2008-2012, 2004.